Properties of a Nanowire Kinetic Inductance Detector Array

Properties of a Nanowire Kinetic Inductance Detector Array

Cite this article as: J. S. Glasby, A. K. Sinclair, P. D. Mauskopf, H. Mani, D. Zhu, M. Colangelo and K. K. Berggren, Properties of a Nanowire Kinetic Inductance Detector Array, Journal of Low Temperature Physics https://doi.org/10.1007/s10909-019-02288-2

Journal of Low Temperature Physics manuscript No.
(will be inserted by the editor)

Properties of a Nanowire Kinetic Inductance Detector Array

J.S. Glasby[1] · **A.K. Sinclair**[2] · **P.D. Mauskopf**[1] · **H. Mani**[2] · **D. Zhu**[3] · **M. Colangelo**[3] · **K.K. Berggren**[3]

the date of receipt and acceptance should be inserted later

Abstract In this paper, we report on the preliminary results of a nanowire kinetic inductance detector, a device which operates as both a standard kinetic inductance detector (KID) and a superconducting nanowire single-photon detector (SNSPD). The device consists of an array of detectors, each with a characteristic resonant frequency which can be readout and distinguished on a single transmission line. We demonstrate, due to the nanowire's small volume, a higher responsivity when operating as a KID under optical loading. Operating the device as an SNSPD, we show the sinusoidal pulse generated from an absorbed photon. Multiple detectors can be struck simultaneously while maintaining the capability to distinguish each pixel. Preliminary results show a variation in count rates among the array, sources are discussed in the text.

Keywords superconducting, nanowire, kinetic inductance, single photon

1 Introduction

Kinetic inductance detectors (KIDs) allow a large number of sensitive superconducting detectors to be readout on a single transmission line. They also provide a relatively simple approach in the fabrication process for large scale arrays. Implementation of KIDs in next-generation astronomical missions [1-4] provides a good foundation for this technology and its development. An array of KIDs can be tuned in such a way that each pixel is associated with a different signal frequency. Many different pixel's signals are combined and readout on one transmission line. The unique resonant frequency of each pixel allows us to differentiate between any in the array.

Superconducting nanowire single-photon detectors (SNSPDs) provide some intriguing properties including low timing jitter ($\sim$ 50 ps), high detection efficiency ($>$ 90%), low dark count rate ($<$ 100 counts/sec), and short reset time ($<$ 50 ns) [5-10]. These qualities

[1]Department of Physics, Arizona State University, Tempe, AZ 85287, USA
[2]School of Earth and Space Exploration, Arizona State University, Tempe, AZ 85287, USA
[3]Department of Electrical Engineering and Computer Science, Massachusetts Institute of Technology, Cambridge, MA 02139, USA
Tel.:(855) 278-5080
E-mail: jglasby@asu.edu

are imperative to many applications a few of which are deep space optical communication, quantum key distribution, and time-correlated single-photon counting.

The device presented in this paper exploits the multiplexing capability of KIDs to build an array of SNSPDs. Recent work has demonstrated the operation of this array with 3 pixels connected [11]. Here we report on the progress of the device as a 12 pixel array. The operation of the array as both a KID and SNSPD is explored and a count rate for each pixel is extracted.

2 Experimental Setup

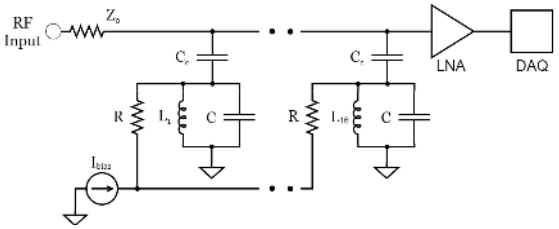

Fig. 1: Circuit diagram of the nanowire kinetic inductance detector array. I_{bias} is the parallel DC bias applied to each nanowire, C and C_c are the tank and coupling capacitors, respectively, Z_0 is the transmission line characteristic impedance 50 Ω, L is the total lumped element inductance which includes geometric and kinetic, R is the DC bias resistor. The transmission line is readout with a low noise amplifier and data acquisition system. The figure has 16 parallel resonators, which correspond to the number fabricated on this chip.

The device presented in this paper was fabricated to take advantage of the low timing jitter of SNSPDs and the multiplexing capability of KIDs [9,12,13]. The inductor chip, which includes a normal inductor and a nanowire meander in series, was fabricated by the Quantum Nanostructures and Nanofabrication Group at MIT. The circuit diagram of the detector with cryogenic LNA is shown in Figure 1, showing several parallel resonators coupled to the transmission line. Although our fabricated device allows up to 16 pixels, 4 were known to disconnected due to the complexity wire bonding to the NbN film. The nanowire meander is identical in each pixel, but the serial inductor varies, tuning the resonant frequency according to $f_0 = 1/2\pi\sqrt{L_T C_T}$, where the total inductance, L_T, is given by the sum of kinetic inductance, L_k, and magnetic inductance, the total capacitance, C_T, is the sum of the resonator capacitor, C, and the coupling capacitor C_c. An actual image of the array is shown in Fig. 2, where the transmission line (c) is connected to SMA pins. Without applying a current bias, the array operates like a KID [14,15]. Incoming photons with sufficient energy to break Cooper pairs in the nanowire, change the kinetic inductance according to $L_k = ml/2e^2 n_{cp} wd$ [16], where m is the mass of the electron, l is the length of the nanowire, e is the electron charge, n_{cp} is the density of Cooper pairs, w and d are the nanowire width and depth, respectively. It is important to note in this configuration a single photon does not turn the nanowire normal, as it does when operating as a single photon detector. Measurements of the change in inductance are shown by a change in resonant frequency and a phase shift. To operate the

device as an SNSPD, the input port is terminated with 50Ω and a DC bias is applied across the nanowires. The current is just below the nanowire's critical current, allowing the array to operate as a single photon detector [17,18]. A photon incident on the nanowire forms a hotspot region, which expands due to Joule heating enveloping the cross sectional area of the nanowire. The normal resistive region generates a voltage pulse in the LC circuit; the pulse is sent down the transmission line, amplified and readout. We can determine which pixel in the array was struck according to the frequency of the signal (i.e. each pixel has its own characteristic frequency). The pulse generated from any pixel will have the same amplitude, but the ringdown time, the time it takes for the signal to decay is longer for lower frequencies. The ringdown is related to the frequency by $\tau = 2Q_r/\omega_0$, where Q_r is the resonator quality factor and ω_0 is the angular resonant frequency. Q_r can be shown to be inversely dependent on the resonant frequency, causing an increase in ringdown time at lower frequencies [15].

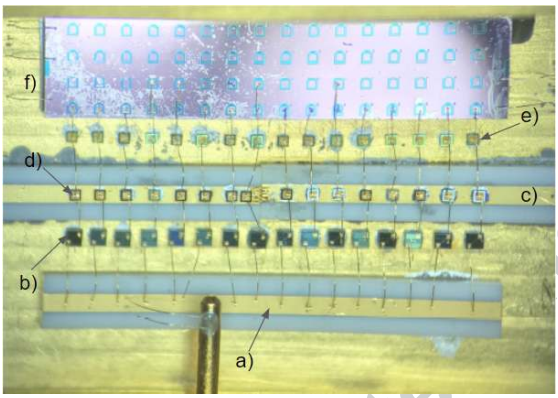

Fig. 2: Device in package with each element connected by an Au wire bond, except for the bond onto the chip which is Al. a) The nanowire current bias line, b) bias line resistor, c) CPW transmission line, d) transmission line coupling capacitor, e) resonant capacitor, f) inductor chip with normal material in series with nanowire meander.

The device was cooled using a Sumitomo RP-082 closed-cycle cryogenic cooler to a base temperature of 3.5 K. A 1300 nm LED was positioned above the array, powered by a Keithley three-channel supply. The probe tone used to read out the resonances is sent and read by an Agilent Vector Network Analyzer (VNA), with a readout power of -90 dBm. The readout power is limited by the critical current for the nanowires, such that a high power could transition the nanowires from a superconducting state to a normal state. The transmitted tone is amplified by a +30 dB LNA at 4 K made at ASU[1]. A 40 dB Mini-Circuits ZKL-1R5+ room temperature amplifier was also used for the single-photon pulses. The nanowires were current biased using a low source Keithley 2400-LV power supply. The single-photon pulses were readout using a Tektronix TDS 7104 Oscilloscope.

[1] http://thz.asu.edu/products.html

3 Results

Once our bath reached a stable temperature of 3.5 K, we measured the resonant frequencies of the array using a VNA. Fig. 3 shows the S21 measurement over the frequency band of interest. Prior to the installation of the device, measurements on the DC bias line revealed 4 pixels were not connected. After cooling down, the missing pixels appear as the large gaps between resonances.

Fig. 4 demonstrates the operation of a single pixel as a KID under optical loading. The intrinsically small volume of the nanowire allows for greater responsivity [19]. Fig. 5 shows a linear relationship between the change in frequency and LED bias current; for a resonant frequency of 123 MHz, this shift corresponds to about 0.5 MHz/mA. Our optical setup for this measurement introduced unwanted thermal loading from the LED. Improvements have been made to fiber couple the LED from a 40 K stage to the device on a 4 K stage.

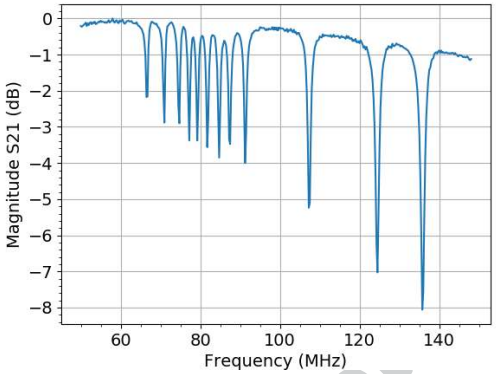

Fig. 3: Transmitted signal of -90 dBm over the frequency band of interest, showing 12 responses. The gaps indicate missing detectors in our array arising from insufficient wire bonds to the chip.

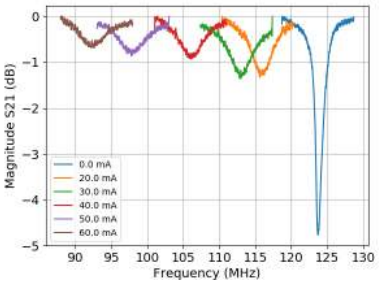

Fig. 4: The shift in resonant frequency at various levels of optical loading.

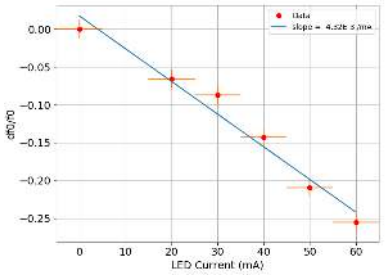

Fig. 5: The linear frequency response of the resonator shown in Fig. 4 as a function of current applied to the LED.

Operating the device as a single photon detector, a 50Ω SMA terminator caps the input port and the nanowires are DC biased just below their critical current, $5\mu A$. The minimum required voltage and current is applied to the LED, illuminating the array. An oscilloscope is used to readout the pulse generated from a single photon event. Fig. 6 shows a timestream of two separate detectors hit simultaneously. The individual signals are superimposed, and the different frequencies create a beating pattern. The Fourier transform of the timestream shown in Fig. 7 demonstrates the imaging capabilities, allowing us to differentiate between pixels.

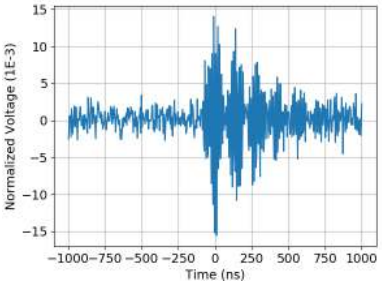

Fig. 6: A timestream of the superposition of two different frequencies indicating two photons triggered different parts of the array. The voltage is normalized to the total voltage of the timestream.

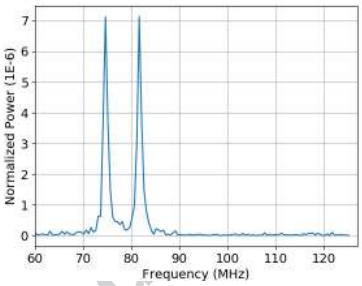

Fig. 7: Taking the Fourier transform of the timestream allows us to determine which detectors were struck by a photon. The normalized voltage pulse was converted into power through the amplifier.

Each voltage pulse has been normalized and converted to power through the readout amplifier. A superimposed image of each event in the frequency domain is shown in Fig. 8, relating the total power sent through the amplifier for each pixel. The higher frequencies have a shorter ringdown time and therefore less power is sent to the amplifier. Comparing this with Fig. 9, we see that this short ringdown time allows for shorter recovery time and higher count rates. There are two factors we think are most likely causing the discrepancy between count rates, 1) the LED is aligned poorly and non-uniformly distributing photons across the array, 2) the intrinsic detection efficiency varies between detectors. Alternative setups have been designed to explore the cause of this discrepancy and will be reported on in the future.

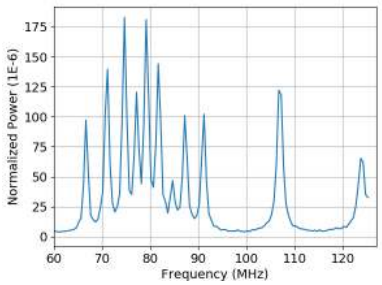

Fig. 8: A superposition of the Fourier transformed timestreams converted into power through the amplifier. The higher frequency detectors have a shorter ringdown time, meaning the power through the amplifier per event is less than the lower frequencies. However, this allows the higher frequency detectors to recover quicker for the next photon event, leading to higher maximum count rates.

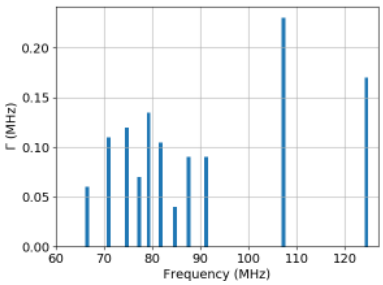

Fig. 9: Count rates acquired per detector. Here we see the higher frequency detectors were struck more regularly, which is expected since the recovery time is less for higher frequencies.

4 Discussion

We have presented an array of single-photon sensitive detectors readout on a single transmission line in a frequency multiplexed scheme developed for KIDs. Development of such a device enables the implementation of SNSPDs in large scale arrays, allowing us to realize some of the potential applications put forward by SNSPDs, including quantum information systems, intensity interferometry, and deep space optical communications. We have shown this device operates as both a KID with high responsivity and an SNSPD with imaging capabilities. Future work on this array includes optimizing optical coupling to the array while mitigating any thermal loading from the LED, development of an FPGA based readout system capable of resolving 100+ pixels, and measuring the arrays intrinsic properties, including timing jitter and system detection efficiency.

References

1. J. Delabrouille, P. de Bernardis, F. Bouchet, A. Achúcarro, P. A. R. Ade, R. Allison et al., *J. Cosmol. Astropart. P.*, **014**, (2018), DOI: 10.1088/1475-7516/2018/04/014.
2. J. E. Austermann, J. A. Beall, S. A. Bryan, B. Dober, J. Gao, G. Hilton et al., *J. Low Temp. Phys.* **193**, 120, (2018).
3. R. Adam, A. Adane, P. A. R. Ade, P. André, A. Andrianasolo, H. Aussel et al., *Astron. Astrophys.* **609**, A115 (2018).
4. N. P. Lourie, P. A. R. Ade, F. E. Angile, P. C. Ashton, J. E. Austermann, M. J. Devlin et al., *Proc. SPIE*, **10708**, 107080L, (2018), DOI: 10.1117/12.2314396.
5. M. J. Stevens, R. H. Hadfield, R. E. Schwall, S. W. Nam, R. P. Mirin, J. A. Gupta, *Appl. Phys. Lett.*, **89**, 031109, (2006), DOI: 10.1063/1.2221516
6. S. Miki, H. Terai, T. Yamashita, , K. Makise, M. Fujiwara, M. Sasaki, Z. Wang, *Appl. Phys. Lett.*, **99**, 111108, (2011) DOI: 10.1063/1.3640503.
7. F. Marsili, V. B. Verma, J. A. Stern, S. Harrington, A. E. Lita, T. Gerrits, S. W. Nam, *Nat. Photonics*, **7**, 210, (2013).
8. K. Smirnov, A. Divochiy, Y. Vakhtomin, P. Morozov, P. Zolotov, A. Antipov, V. Seleznev, *Supercond. Sci. Tech.*, **31**, 035011, (2018).
9. W. Zhang, L. You, H. Li, J. Huang, C. Lv, L. Zhang, X. Xie, *Sci. China Phys. Mech.*, **60**, 120314, (2017).
10. I. Holzman, Y. Ivry, *Adv. Quantum Technol.* **2**, 1800058, (2019), DOI: 10.1002/qute.201800058.
11. A. K. Sinclair, E. Schroeder, D. Zhu, M. Colangelo, J. Glasby, P. D. Mauskopf, H. Mani, K. K. Berggren, *IEEE T. Appl. Supercon.*,**29**, (2019), DOI: 10.1109/TASC.2019.2899329.
12. N. Calandri, Q. Y. Zhao, D. Zhu, A. Dane, K. K. Berggren, *Appl. Phys. Lett.*, **109**, 152601, (2016), DOI: https://doi.org/10.1063/1.4963158.
13. B. A. Korzh, Q. Y. Zhao, S. Frasca, et al. *arXiv preprint*, **1804.06839**, (2018).
14. J. Zmuidzinas, *Annu. Rev. Condens. Matter Phys.*, **3**, (2012), DOI: 10.1146/annurev-conmatphys-020911-125022.
15. P. D. Mauskopf, *Publ. Astron. Soc. Pac.*,**130**, 082001, (2018).
16. A. J. Annunziata, D. F. Santavicca, L. Frunzio, G. Catelani, M.J. Rooks, A. Frydman, D.E. Prober, *Nanotechnology*, **21**, 445202, (2010).
17. J. K.Yang, A. J. Kerman, E. A. Dauler, V. Anant, K. M. Rosfjord, K. K. Berggren, *IEEE T. Appl. Supercon.*, **17**, (2007).
18. C. M. Natarajan, M.G. Tanner, R.H. Hadfield, *Supercond. Sci. Tech.*, **25**, 063001, (2012).
19. S. Doyle, P. D. Mauskopf, J. Naylon, A. Porch, C. Duncombe, *J. Low Temp. Phys.*, **151**, (2008), DOI: 10.1007/s10909-007-9685-2.